RSC Advances

Development of composite anion-exchange membranes using poly(vinyl alcohol) and silica precursor for pervaporation separation of water-isopropanol mixtures

Journal:	*RSC Advances*
Manuscript ID	RA-ART-09-2015-019858.R1
Article Type:	Paper
Date Submitted by the Author:	05-Jan-2016
Complete List of Authors:	H. G., Premakshi; Karnatak University, Dharwad, Department of Chemistry Kariduraganavar, Mahadevappa; Karnatak University, Dharwad, Department of Chemistry Mitchell, G; Centre for Rapid and Sustainable Product Development, Campus 5, Rua das Olhalvas, 2414-016, Leiria, Portugal,, Politechnique Institute of Leiria,
Subject area & keyword:	Films/membranes < Materials

Development of composite anion-exchange membranes using poly(vinyl alcohol) and silica precursor for pervaporation separation of water-isopropanol mixtures

H. G. Premakshi[1], M. Y. Kariduraganavar[1*], G. R. Mitchell[2]

[1]*Post-Graduate Department of Studies in Chemistry, Karnatak University, Dharwad-580 003, India*

[2]*Centre for Rapid & Sustainable Product Development, Polytechnic Institute of Leiria, Leiria-2430 028, Portugal*

ABSTRACT

Composite anion-exchange membranes were prepared using sol-gel techniques with poly(vinyl alcohol) (PVA) and anion-exchange silica precursor (AESP). Ammonium functionality was created on the AESP through a ring opening reaction between 2-(3-aminoethylamino)propyltrimethoxysilane and glycidyltrimethylammonium chloride under mild heating conditions. The resulting membranes were subjected to physico-chemical investigations using various techniques. The pervaporation performance of the membranes was systematically investigated based on the effects of feed composition and the mass% of AESP. Among the membranes studied, the membranes containing 4 mass% of AESP exhibited the highest separation factor of 2,991 with a flux of 10.76×10^{-2} kg/m^{2}h at 30 °C for 10 mass% of water in the feed. The trade-off phenomenon which exists between the flux and the separation factors was overcome by the incorporation of AESP in PVA matrix. We find that the overlap between the total flux and flux of water, suggests that these membranes could be used effectively to break the azeotropic point of water-isopropanol mixtures. From the temperature dependent diffusion and permeation values, the Arrhenius activation parameters were estimated. The E_p and E_D values ranged between 18.36 and 7.94, and 18.68 and 8.09 kJ/mol, respectively. The negative heat of sorption (ΔH_s) values was obtained for all the membranes, indicating that Langmuir's mode of sorption is predominant in the transport process.

Keywords: Poly(vinyl alcohol); Anion-exchange silica precursor; Isopropanol; Pervaporation; Activation energy.

*Corresponding Author: Dr. M. Y. Kariduraganavar (mahadevappayk@gmail.com)
Fax: +91-836-2771275; Phone: +91-836-2215286 Extn. 23.

1. Introduction

Pervaporation (PV) has gained widespread acceptance within the chemical industries as an effective membrane based process for the separation of azeotropic and close boiling liquid mixtures.[1-4] In particular, great efforts have been made to develop effective membranes for the dehydration of alcohols such as ethanol and isopropanol.[5-8] For the dehydration process, hydrophilic polymer membranes are the choice for the selective removal of water from the organic phase. Thus, the development of a commercial feasibility for the PV process largely depends on selection of membrane material and its properties.[9-12]

The study of the PV process started with poly(vinyl alcohol) (PVA) as the membrane material, and it has continued to be widely studied for membrane applications owing to its unique properties such as high hydrophilicity, film forming ability and good chemical stability. Unfortunately, it has certain inherent drawbacks; mainly excessive swelling in aqueous solution. This leads to a lower selectivity and an unfortunate trade-off between separation factor and permeation flux. To circumvent this problem, several researchers have tried to modify the PVA through crosslinking, blending, grafting, etc.[13-15] None of these modifications improves the PV performance as was expected.

New composite membranes have been recently reported which were developed by combining organic and inorganic materials in particular ratios, which offered specific advantages in terms of the dehydration of alcohols with desirable thermal and chemical stability. This type of modification provides a possible facile and feasible way to solve the

trade-off phenomenon, which generally exists in all PV processes. Our research group[16] recently developed TiO_2 incorporated composite chitosan membranes which were able to increase both flux and separation factors simultaneously for the dehydration of isopropanol. Among the developed membranes, the membrane containing 40 mass% of TiO_2 exhibited the highest flux of 0.15 kg/m^{2}h with a separation factor of 4,728 at 30 ^oC for 10 mass% of water in the feed. Zhou et al.[17] developed SiO_2/PDMS hydrophobic membranes with different substrates, and increased both flux and separation factor simultaneously by suitably modifying the surface properties of the membranes. For 5.5 mass% of ethanol, membrane with PVDF substrate exhibited 5.9 separation factor with a flux of 0.59 kg/m^{2}h at 40 ^oC. Novel sodium alginate membranes were developed by Sajjan et al.[18] through the incorporation of chitosan-wrapped multi-walled carbon nanotubes (MWCNTs) into the membranes, which led to an increase of both the permeation flux and separation factor for the dehydration of isopropanol at 30 ^oC. Membrane with 2 mass% of MWCNTs demonstrated an excellent flux of 0.22 kg/m^{2}h with a separation factor of 6,420 at 10 mass% of water in the feed. In that work, the way in which the hard material was incorporated into the soft matrix materials was really appreciable, and this has provided a new route for the synthesis of PV membranes for the effective separation of aqueous-organic mixtures.

In our previous study,[12] we followed this new approach for the development of nanocomposite membranes via in-situ preparation of silver nanoparticles in PVA matrix which increased both the factors simultaneously. Membrane with 2 mass% of AgNps exhibited an excellent flux of 0.072 kg/m^{2}h with a separation factor of 634 at 10 mass% of water. Modified composite chitosan membranes were also developed using NaY zeolite and which have exhibited simultaneous increase in both flux and separation factor[19], and particularly

membrane having 40 mass% of NaY zeolite shown an excellent flux of 0.114 kg/m^{2}h with a separation factor of 11,241 at 10 mass% of water for 30 ^{o}C. Using a similar strategy, very recently Pan[20] and our group[21] reported novel nanocomposite membranes composed of PVA and chitosan-wrapped carbon nanotubes, and TGDMP incorporated chitosan membranes, respectively. At 30 ^{o}C, chitosan-wrapped membrane containing 1 mass% CNT-CS has shown an excellent flux of 0.066 kg/m^{2}h with a separation factors of 53 at 10 mass% water. However, for the same mass% of water, membrane having 1.2 mass% of TGDMP demonstrated a flux of 0.102 kg/m^{2}h with a separation factor of 591.

An alternative approach involves ion-exchange membranes prepared from various hydrophobic backbones which can play a unique role as pervaporation membranes. In fact, ion-exchange membranes have been recently explored for electrodialysis and fuel cell applications.[22-25] The balance between the hydrophobicity and hydrophilicity of such ion-exchange membranes are generally controlled by the degree of crosslinking and the level of sulphonation/quaternization. Zhang et al.[9] developed quaternized PVA membranes with a flux of 12.63 kg/m^{2}h and a separation factor around 58. The same group[26] developed quaternized membranes using PVA and APTEOS, and achieved an insignificant flux of 0.036 kg/m^{2}h with a separation factor of 537. Similarly, Meng et al.[27] and Sajjan et al.[28] prepared amino functionalized PVA membranes using TEOS and obtained a flux of 1.1 kg/m^{2}h and separation factor 700, and quaternized PVA membranes using GTMAC with a flux of 1.92 kg/m^{2}h and separation factor 1570. All these ion-exchange membranes exhibited excellent mechanical and chemical stability, but failed to increase both the flux and the separation factors simultaneously, which is a critical step for making the PV process commercially viable.

In light of this understanding, we have set out to develop novel ion-exchange membranes with the prime aim of increasing both the permeation flux and the separation factor. To address this challenge, we start with the low cost PVA material which is quaternized with an anion-exchange silica precursor prepared via an electrophilic ring opening reaction between 3-(2-aminoethylamino)propyltrimethoxysilane (APTMS) and glycidyltrimethylammonium chloride (GTMAC). The physico-chemical properties of the resulting membranes were studied with various techniques, and evaluated for PV separation at different temperatures and feed compositions. The performance of the membranes is discussed by correlating the values of separation factor and the permeation flux with the structure of the membrane material. From the temperature dependence of the permeation flux and the diffusion coefficients, the Arrhenius activation parameters were estimated. These results are discussed in terms of PV separation efficiency of the membranes.

2. Experimental

Materials

Poly(vinyl alcohol) ($\bar{M}_w$ ~ 125,000), 3-(2-aminoethylamino)propyl trimethoxysilane and glycidyltrimethylammonium chloride were procured from E. Merck Ltd., Mumbai, India. Isopropanol, formaldehyde and sulphuric acid were purchased from s. d. fine Chemicals Ltd., Mumbai, India. All the chemicals were of reagent grade and used without further purification. Water was deionized and distilled before use.

Synthesis of anion-exchange silica precursor

The anion-exchange silica precursor was synthesized using epoxide ring opening reaction. In a typical synthetic procedure, 1:1 mole ratio of APTMS and GTMAC were mixed at room temperature and subjected for stirring at 80 ^{o}C for 6 h. A transparent AESP solution was

obtained. These AESP–PVA composite anion-exchange membranes were prepared using a sol-gel technique in acidic medium followed by crosslinking of –OH groups via the formal reaction shown in Fig. 1.

Membrane preparation

Poly(vinyl alcohol) (4 g) was dissolved in 100 ml of deaereated distilled water under constant stirring for ~24 h at room temperature. While stirring, the PVA based mixture was crosslinked by adding 1ml of formaldehyde and 1ml of 0.2 M of sulphuric acid as a catalyst. The resulting mixture was left overnight so as to remove the air bubbles. The clear solution was cast onto a glass plate and dried for 2-3 days at ambient temperature to yield a film of uniform thickness. The dried membrane was peeled-off and annealed at 60 $^{\circ}$C for 24 h in an inert atmosphere in order to activate the cross-linking process and was designated as membrane M.

To prepare the composite membranes, the desired quantity of AESP was added into the above clear solution and stirred for 2 h and then the procedure described above was followed as for membrane M. The amount of PVA was kept constant for each membrane. The amount of AESP with respect to PVA was varied as 1, 2, 3 and 4 mass%, and the membranes thus obtained were designated as M-1, M-2, M-3 and M-4, respectively. The thickness of the membranes was found to be 40 ± 2 μm measured using a peacock dial thickness gauge (Model G, Ozaki MFG. Co. Ltd., Japan).

Fourier transform infrared (FTIR) spectroscopy

The IR spectra of crosslinked PVA and its composite membranes were recorded using FTIR spectrometer (Nicolet, Impact-410, USA) in the range of 400 to 4000 cm^{-1}. Samples were prepared by grinding films cooled with liquid nitrogen to a powder which was mixed with KBr

and then compressed into discs. In order to estimate the changes in the intensities of the characteristic peaks with respect to the amount of AESP, the amount of membrane sample and KBr were kept constant in each scan.

Wide-angle X-ray diffraction (WAXD)

The X-ray diffraction profiles of the membranes were recorded at room temperature using a Brucker D-8 advanced wide-angle X-ray diffractometer operating in reflection mode. The X-ray source was Ni-filtered Cu Kα radiation (40 kV, 30 mA). The membranes of uniform thickness (40 ± 2 μm) were mounted on a sample holder and the patterns were recorded over a range of 2θ from 5 to 50° with a speed of 8°/min.

Differential scanning calorimetry (DSC)

The glass transition temperatures of the membranes were recorded using a differential scanning calorimeter (DSC Q 20, TA Instruments, Waters LLC, USA) with a heating rate of 10 ºC/min under a nitrogen atmosphere and a sample mass of 6-9 mg.

Thermogravimetric analysis (TGA)

All the membranes were subjected to thermogravimetric analysis (DSC Q20, TA Instruments, Waters LLC, New Castle, Delawave, USA) with a heating rate of 10 °C/min under nitrogen atmosphere and with a sample mass of 8-10 mg.

Scanning electron microscopy (SEM)

The surface and cross-section views of the membranes were recorded using scanning electron microscope (JEOL, JSM-400 Å, Tokyo, Japan). All specimens were coated with a conductive layer (400 Å) of sputtered gold. The cross-sections were prepared by sectioning the film using a sharp razor blade.

Mechanical properties

The mechanical properties such as tensile strength and percent elongation at break of the resulting membranes were measured at 25 ºC by employing a standard ASTM D 638 method using and Universal Testing Machine (Hounsfield, H25KS, UK) with a crosshead speed of 50 mm/min. During the measurement, the relative humidity was maintained between 55 and 60%. Prior to this, the membranes were stored in a WT Binder for 24 hrs with constant temperature (25 ^{o}C) and humidity (55-60%). For each sample, five specimens were tested and results are presented as an unweighted average.

Swelling measurements

Each membrane was dried using an electronically controlled oven (WTB Binder, Jena, Germany) at a temperature 50 °C for 2 hours and then its mass was obtained using a digital microbalance (Mettler, B204-S, Toledo, Switzerland) within an accuracy of ± 0.01 mg. The membranes were equilibrated by soaking in different compositions of water-IPA mixtures in sealed vessels at 30 ºC for 24 h. The swollen membranes were removed and weighed as quickly as possible (after careful blotting). The percent degree of swelling (*DS*) was calculated as:

$$DS\,(\%) = \left(\frac{W_s - W_d}{W_d} \right) \times 100 \qquad (1)$$

where W_s and W_d are the weight of swollen and dried membranes, respectively.

Ion-exchange capacity

The ion-exchange capacity was measured using a classical titration method. Initially all the composite membranes were immersed in distilled water for 2 h, and subsequently they were

soaked in 100 ml of 0.1 M NaOH for 12 h to convert them into OH^- forms. Then they were washed with deionized water to remove excess NaOH and then equilibrated with 25 ml of 0.1M HCl solution for 24 h. The ion exchange capacity (IEC) of the membranes was determined from the reduction in acid measured using back titration. The IEC values were obtained from the following equation:

$$IEC(mequiv.g-1) = \frac{M_{o,}HCl - M_{e,}HCl}{m_d} \quad (2)$$

where M_o, HCl is the milliequivalents of HCl required before equilibrium, M_e, HCl is milliequivalents of HCl required after equilibrium, and m_d is the mass (g) of the dried membrane.

Pervaporation experiments

The pervaporation experiments were carried out using the apparatus shown in Fig. 2. The membrane under test was mounted in the stainless steel pervaporation unit. The effective area of the membrane in contact with the feed mixture was 34.23 cm^2 and the capacity of the feed-side of the unit was about 250 cm^3. The temperature of the feed was maintained at set temperature in the range 30-50 ºC by circulating the water through the cell jacket from a temperature controlled bath. For all the measurements, the downstream pressure was maintained at 10 Torr (1.333224×10^3 Pa) using a two-stage vacuum pump (Toshniwal Instruments, Chennai, India). The water composition in the feed mixture of water/isopropanol was varied from 10 to 30 mass%. The system was conditioned for 2 h to allow the membrane to reach equilibrium before collecting any permeate. While running the PV experiment, the permeate was condensed in a cold trap immersed in liquid nitrogen and collected at regular intervals over 1 h. The experiments were carried out at 30, 40 and 50 °C. The collected

permeate was measured using a digital microbalance. The proportions of water and isopropanol in the permeate were estimated by measuring the refractive index of the liquid within an accuracy of ± 0.0001 units using an Abbe refractometer (Atago-3T, Japan) and then reading off the composition from a standard graph, that was previously constructed using known compositions of water-isopropanol mixtures. All the experiments were performed at least three times and the results are presented as an unweighted average. This procedure proved to be very consistent within ± 4% of the range plotted.

Based on the amount of permeate and the compositions, the flux (J) and separation factor (α) were calculated using the following equations:

$$J = \frac{W}{A.t} \tag{3}$$

$$\alpha_{sep} = \frac{P_w / P_{IPA}}{F_w / F_{IPA}} \tag{4}$$

where W is the total mass of permeate collected at time t (h); A is the area of the membrane. Subscripts w and IPA refer to the components of water and isopropanol, respectively, while P and F are the weight fractions of permeate and the feed, respectively.

3. Results and Discussion

Synthesis of membrane

Prior to the preparation of the PVA-AESP composite membranes, the AESP was hydrolyzed in the presence of an acid catalyst leading to the formation of silanol groups. The resulting silanol groups are dispersed through the PVA based system, the –OH groups of silanol formed siloxane bonds with another silanol or with -OH groups of PVA through dehydration or dealcolysis reaction during the membrane drying stage. In addition, the -OH and NH_2 groups

present in the AESP can form hydrogen bonds with the -OH groups of PVA. These hydrogen and siloxane bonds act as crosslinks in the resulting hybrid membranes. Eventually as the fraction of cross-linking increases, these crosslinks will suppress the mobility of the PVA chains and thereby the stability and the density of the membrane could be increased.[29]

Membrane characterization

FTIR Studies

Figure 3 illustrates the FTIR spectra of PVA and the range of composite membranes. The membrane M exhibited a characteristic band at around 3400 cm^{-1} and multiple bands between 900 and 1200 cm^{-1}, which correspond to the –OH and C-O/Si-O stretching vibrations. Upon developing the ion-exchange membranes by incorporating anion-exchange silica precursor via *in-situ* method in the PVA matrix, the intensity of the –OH band did not change appreciably. We attribute this to the simultaneous consumption and creation of –OH groups, resulting in a constant OH composition in the PVA matrix. This does not mean that the hydrophilicity of the membrane has been degraded as the hydrophilicity of the membranes in this study is mainly due to the creation of quaternary ammonium groups, with the increasing silica precursor in the matrix. This is can be seen from the bands which appeared at around 950, 1480 and 2940 cm^{-1}, and which are assigned to the quaternary ammonium groups present in AESP.[28,30] The stretching vibrations appeared at 2979 and 1033 cm^{-1} are assigned to $–CH_3$ groups (asymmetric stretching vibrations) and these are in good agreement with data reported by Kumar et al.[31]

An unusual band was appeared at around 1700 cm^{-1} in membrane M. This is the carbonyl band (C=O) of formaldehyde that was added in the case of the PVA only membrane to crosslink the polymer. The formaldehyde was added with a sole intention to facilitate the comparison of the PVA membranes with the resulting composite membranes. However, the

intensity of this band (1700 cm^{-1}) decreased as the content of anion-exchange silica precursor was increased. This indicates that the consumption of formaldehyde available for the crosslinking reaction decreased as the mass% of the silica precursor was increased. This shows that the anion-exchange precursor reacted with the PVA in presence of acid catalyst yielding crosslinked anion-exchange membranes.

WAXD Studies

To examine the crystallinity of the composite membranes, the X-ray diffraction measurements were performed and the patterns obtained are presented in Fig. 4. It is observed that the diffraction pattern of the crosslinked PVA membrane exhibited a typical pattern for a semi-crystalline polymer with a sharp peak at around $2\theta = 20^{o}$, which can be assigned to a mixture of (101) and (200) crystalline planes[13] superimposed on a rather broad peak corresponding to the amorphous component. However, as the content of AESP was increased from membrane M-1 to M-4, the intensity of the peak at 20° decreased. This suggests that the fraction of crystalline domains is reduced in the composite membrane matrix. We attribute this is to the hydrogen bonding and the interaction between the –OH groups of PVA and silanol, and the quaternary ammonium groups of AESP[32] which will increase as the content of AESP was increased. This leads to an increase of the amorphous fraction, which generally favors the diffusion of permeants through the membrane.

DSC Studies

Figure 5 shows the DSC thermograms of the crosslinked PVA and the composite anion-exchange membranes. The feature observed at around 100 °C, corresponds to the glass transition (T_g) and this slightly increased with increasing AESP content in the crosslinked

PVA matrix and a value of 110 ºC was recorded for the membrane with a AESP content of 4 mass%. This is due to the formation of the network structure between AESP and PVA.

A strong endothermic peak was observed at 186 °C for the crosslinked PVA membrane which is typical of partially hydrolyzed PVA and corresponds to the melting point (T_m) of the crystalline domains. The observed peak value gradually increased to 225 °C with increasing the AESP content. The higher value of T_m is typical of a fully hydrolyzed PVA due to the increased number of OH groups. The fact that the X-ray diffraction patterns are very similar to PVA suggests that the crystalline domains are largely formed of PVA sequences. The invariance in the peak position and full width at half height in the X-ray diffraction patterns with changing AESP content suggests that the regions of the PVA molecule which have reacted with the AESP are not incorporated in to the crystal structure as might be expected. There is a significant jump in the value of T_m between membranes M to M-1; the higher AESP content membranes M-3 and M-4 exhibit a slightly lower T_m although this still above the values exhibited by membrane M. This slight shift downwards can be attributed to the reducing crystal size as the fraction of the non-crystallisable crosslinked PVA increases. We attribute the jump in T_m for membranes involving ASEP to the formation of strong inter- and intramolecular interactions in the amorphous component close to the crystal surface owing to the presence of quaternary ammonium and polar -OH groups.

TGA Studies

The TGA curves of crosslinked PVA and the composite membranes are shown in Figure 6. The thermograms exhibit a two step weight loss. In the first step (ambient to 125 °C), there is small weight loss of ~15 to 20% which we relate to the loss of absorbed water molecules. The second step, from 200 to 475 ºC, involves a much larger loss, which is attributed to degradation

of the quaternary ammonium groups and the crosslinked membrane matrix.[33] No further decomposition was observed beyond 475 °C, but we note that the overall percent decomposition was lower as the content of AESP was increased. This further supports the view that the functionalized silica precursor improves the thermal stability of the membranes.

SEM Studies

The microscopic morphologies of the crosslinked PVA and the composite membranes are shown in Figure 7. It can be observed from Figure 7A that the surfaces of all the membranes are smooth; no voids are seen. Figure 7B shows the cross-section morphologies of the membrane with high resolution. It can be seen that small circular crater-like structures are on the surface for all the membranes which reflects the preparation procedure for the section. There is no evidence for any phase separation in these low magnification micrographs of the composite membranes, and so we speculate that the AESP is distributed in the PVA matrix homogeneously. A uniform distribution of silica particles in the polymer matrix would assist in promoting ionic transport and thereby increase water permeation through the membrane.[33]

Tensile properties

The tensile strength and percent elongation of a membrane inform on its suitability for PV applications. The effect of AESP on the tensile strength and percent elongation of the membranes were studied and the data obtained are reported in Table 1. This shows that the tensile strength increased from 54 to 69 MPa with increasing AESP content in the membranes. However, we also note that with increasing the content of AESP the percent elongation was decreased from 90 to 45. It is due to the contribution of electrostatic interaction, hydrogen and covalent bonding established in the composite membranes and thus these observations match our expectations.

Ion-exchange capacity

The ion-exchange capacity (*IEC*) of crosslinked PVA and its composite membranes are also included in Table 1. The *IEC* values are related to the number of accessible and exchangeable hydrophilic groups grafted onto the membrane matrix, which are responsible for their charged nature. It is observed that *IEC* values of the membranes increased from 0.25 to 0.73 (meq/g) with increasing AESP content in the crosslinked PVA membranes. This clearly shows that the incorporation of AESP into the PVA matrix increased the number of charged quaternary ammonium ($N^+(CH_3)_3$) groups; this will be important for the selective transport of aqueous permeants across the membrane.

Effects of feed composition and AESP content on membrane swelling

The sorption mechanism depends on the structure of the membrane, the affinity of the permeants towards the membrane, and the reciprocal interaction between the permeants.[34,35] In the PV process, the membrane sorption plays a key role in the separation performance of the membrane, which is generally assessed by studying the membrane swelling in different feed mixtures. Figure 8 shows the swelling performance of all the membranes in differently feed mixtures of water and IPA at 30 ºC. It is observed that the degree of swelling increased almost linearly for all the membranes with increasing the water composition in the feed. This is due to the increased interaction between water molecules and the membrane, owing to the presence of the large number of interactable hydrophilic groups (-OH, -NH, silanol, and $N^+(CH_3)_3$) in the membrane matrix. This is in line with expectations as water is more polar than IPA, and it preferentially interacts with the hydrophilic groups of the membrane, resulting in an increased degree of swelling. It is also observed that the degree of swelling of the composite membranes is greater than that of the crosslinked PVA membrane (M). This is because, the inclusion of the

AESP results in a higher degree of the amorphous domain in the membrane as shown from X-ray data. Furthermore the composite membranes are more hydrophilic than the membrane M due to the presence of a large number of quaternary ammonium groups of AESP in the composite membranes. Accordingly, the degree of swelling was increased with increasing the AESP content in the membrane matrix (M-1 to M-4). In addition, the formation of hydrogen bonding becomes more predominant in the membrane matrix as the content of AESP was increased in the composite membrane. This reduces the fraction of crystallisable PVA molecules existing in the crosslinked PVA matrix and accordingly the crystallinity of the crosslinked membrane is reduced. Clearly, the change in the membrane structure and the increased interaction between the permeants and the membrane are together responsible for the enhanced degree of swelling with increasing the AESP content in the crosslinked membrane matrix.

Effects of feed composition and AESP content on pervaporation performance

Figure 9 demonstrates the effects of the feed composition and the AESP content on the total permeation flux for all the membranes at 30 ºC. It is found that the total permeation flux increased linearly with increasing water composition in the feed. This mirrors the results observed in the swelling study (Fig. 8). Principally this is because of increased interactions between the water molecules and the membrane, since the membranes have a large number of hydrophilic groups such as -OH, -NH, silanol, and quaternary ammonium. Particularly, the permeation flux of the composite membranes was greater than that of the crosslinked PVA membrane (M), and increased with respect to the amount of AESP content in the membrane. This is because of increased interactable groups in membrane such as -OH, -NH, silanol and -$N^{+}(CH_3)_3$. These are responsible for the reduction in the crystallinity in the membrane matrix

as shown from the X-ray results. As a result, the membranes exhibit a greater interaction with the permeants and thereby increase the permeation flux significantly from membrane M to M-4.

In order to assess the separation performance of the membranes, we have calculated the separation factor for all the membranes at 30 °C for different compositions of the feed fluid in the pervaporation unit and these values are presented in Fig. 10. It is observed that separation factor decreases exponentially with an increasing water composition in the feed liquid. We propose that when there is an interaction between the membrane and a highly polar solvent like water present in the membranes, the polymer chains tend to relax greatly and thereby the selectivity of the membrane reduces. On the other hand, the separation factor was increased with increasing the AESP content in the membranes; this effect is more prominent at lower compositions of water in the feed. This is mainly a consequence of the lower water composition, wherein relaxation of polymer chains is less predominant. Secondly, as explained in Fig. 9, groups such as –OH, -NH, silanol and $-N^{+}(CH_3)_3$ present in the membranes are increased with increasing the AESP content in the membrane and make the membranes more hydrophilic. Consequently, at a fixed water composition membranes with higher amount of the AESP facilitate a greater selectivity.

This is further demonstrated in Fig. 11, in which both the flux and the separation factors are plotted as function of the AESP content in the membranes for a feed liquid containing 10 mass% of water. It is striking to observe that both the permeation flux and the separation factor were increased simultaneously with increasing the AESP content in the membrane. This is an uncommon observation due to the more common trade-off phenomenon existing between the flux and the separation factors in the PV process. However, the creation of a large number

of hydrophilic quaternary ammonium groups through the incorporation of the AESP content, establishes electrostatic interactions and hydrogen bonding within the membrane matrix which overcome the phenomenon. This is an important step as it has been the limiting factor for the commercial utilization of the PV process. Generally, when a polymer is crosslinked the separation factor increases, but the flux decreases. In contrast in the present study, we have increased both the flux and the separation factor simultaneously by judiciously introducing the quaternary ammonium groups in the crosslinking segment.

To assess the overall PV performance of the membranes, we have calculated the individual fluxes as a function of mass% of the AESP content at 10 mass% of water in the feed and the data are presented in Fig. 12. It is clearly observed that the total flux and flux of water are overlapping with each other. As can be easily observed, the flux of isopropanol is negligibly small, suggesting that the membranes developed in the present study through the incorporation of the AESP content are highly selective towards the water with a substantial improvement in the flux compared to the crosslinked membrane M. Among the membranes discussed here, the membrane containing 4 mass% of AESP demonstrated an excellent flux of 10.76×10^{-2} kg/m^{2}h with a separation factor of 2,991 at 30 °C for 10 mass% of water in the feed.

Diffusion coefficient

The mass transport of binary liquid molecules through a polymer matrix is generally explained by the solution-diffusion mechanism, which occurs in three steps: sorption, diffusion and evaporation.[36] Thus, the permeation rate and separation factor are governed by the solubility and diffusivity of each component of the feed to be separated. In the PV process, because of the establishment of a fast equilibrium distribution between the bulk feed and the upstream

surface of a membrane, the diffusion step controls the transport of penetrants[37] It is therefore important to estimate the diffusion coefficient, D_i of penetrating molecules to understand the mechanism of transport. Thus, diffusion coefficient D_i was calculated from the experimental data shown earlier using a modified Fick's equation reported previously.[38,39] The calculated values of D_i at 30 °C are presented in Table 2. It is observed that the diffusion coefficient of water is noticeably increased from M to M-4 while simultaneously the diffusion coefficients of IPA are depressed. This trend remains same for all the membranes at all water compositions in the feed.

On the contrary, the diffusion coefficient of water was marginally decreased for all the membranes except membrane M with increasing water in the feed liquid. In contrast, the diffusion coefficient of IPA was significantly increased with increasing the water concentration in the feed for all the membranes. Nevertheless, the magnitude of diffusion coefficients of water was substantial in comparison with that of isopropanol, demonstrating that the membranes developed in the present study are highly selective towards water.

Effect of temperature on membrane PV performance

The effect of the operating temperature on the PV performance for water-isopropanol mixtures was studied for all the membranes at 10 mass% of water in the feed, and the values obtained are presented in Table 3. It is noticed that with increasing temperature the rate of permeation was increased for all the membranes, while decreasing the separation factor. Generally, this happens because of two reasons. First, as the temperature increases the vapour pressure difference between the upstream and downstream side of the membranes increases and this in turn enhances the driving force. Second, an increase of temperature promotes the thermal motion of polymer chain segments, creating more free-volume in the polymer matrix.

Although, in the present study the experiments were performed well below the glass transition temperature of PVA,[8] but of course the membranes are highly swollen and we might expect this second factor to be of limited significance. Therefore, the vapour pressure difference played a major role in transporting the associated molecules along with the selective permeants. This gives rise to an increase of total permeation flux while suppressing the selectivity. Thus, the temperature dependence of permeation and diffusion has prompted us to estimate the activation energies for permeation and diffusion using the Arrhenius type equation[40,41]:

$$X = X_o \exp\left(\frac{-E_x}{RT}\right) \tag{5}$$

where X represents permeation (J) or diffusion (D). X_o is a constant representing pre-exponential factor of J_o or D_o. E_x represents the activation energy for permeation or diffusion depending on the transport process under consideration, and RT is the usual energy term.

Arrhenius plots of log J and log D versus temperature are shown in Figs. 13 and 14. In both the cases, a linear trend was observed, suggesting that the permeability and diffusivity follow a largely Arrhenius trend. We have estimated the activation energies for total permeation (E_p) and diffusion (E_D) using least-squares fits of these linear plots. Similarly, the activation energies for the permeation of water (E_{pw}) and isopropanol (E_{pIPA}) were estimated, but the plots are not given to minimize the figures. However, the values thus obtained are tabulated in Table 4.

From Table 4, it is observed that the apparent activation energy values for water permeation (E_{pw}) are lower than those of isopropanol permeation (E_{pIPA}), and the difference between these two was significantly increased from 4.66 to 31.50, suggesting that membranes

developed with the higher amounts of AESP demonstrated excellent separation efficiency towards water. The activation energy values for water permeation (E_{pw}) and total permeation (E_p) are almost close to each other, signifying that coupled-transport of both water and isopropanol is minimal as due to higher selective nature of the membranes. It is further noticed that as the AESP content was increased in membrane M-1 to M-4, the activation energy values of both E_p and E_D were systematically decreased. This is due to increased hydrophilicity by the incorporation of AESP content in the membrane matrix, and apparently the energy required for transport of selective permeants was reduced. The estimated E_p and E_D values ranged between 18.36 and 7.94, and 18.68 and 8.09 kJ/mol, respectively. Using these values, we have calculated the heat of sorption as

$$\Delta H_s = E_p - E_D . \quad (6)$$

The resulting ΔH_s values are included in Table 4. The ΔH_s values give the additional information about the transport of molecules through the polymer matrix. It is a composite parameter involving the contributions of both Henry's and Langmuir's mode of sorption.[42] Henry's law states that the heat of sorption is positive for liquid transport, leading to the dissolution of chemical species into a site within the membrane, giving an endothermic contribution to the sorption process. However, Langmuir's sorption requires the pre-existence of a site in which sorption occurs by a hole filling mechanism, giving an exothermic contribution. The ΔH_s values obtained in the present study are negative, indicating that Langmuir's mode of sorption becomes predominant.

4. Conclusions

In the present study, anion-exchange membranes were developed using PVA and AESP with ammonium functionality using the ring opening of GTMAC under mild heating conditions. We have shown that increasing the AESP content results in a simultaneous increase of both the permeation flux and the selectivity. This was explained on the basis of the enhancement of the hydrophilic character and increased rigidity of the membrane due to a greater interaction between PVA and AESP. The experimental data also reveal that the total flux and flux of water are closed to each other for all the membranes, showing that the developed membranes are highly selective towards water. Among the membranes developed, the membrane containing 4 mass% of AESP demonstrated the highest separation factor of 2,991 with a flux of 10.76×10^{-2} kg/m^{2}h. With an increase in temperature, the permeation flux was increased while decreasing the separation factor and this was attributed to the vapour pressure difference created between the upstream and the downstream side of the membrane. The ΔH_s values obtained in the present study are negative for all the membranes, suggesting that sorption occurs only by hole-filling mechanism, and involving Langmuir's mode of sorption. The high flux and high selectivity factor make these membranes particularly suitable for utilization in commercial scale separation processes.

Acknowledgements

GRM acknowledges the support of the FCT (Portugal) in completing this work.

References

1 R. Y. M. Huang (Ed.), Pervaporation Membrane Separation Processes, Elsevier, Amsterdam, 1991.

2 P. Shao and R. Y. M. Huang, J. Membr. Sci., 2007, 287, 162–179.

3 P. D. Chapman, T. Oliveira, A. G. Livingston and K. Li, J. Membr. Sci., 2008, 318, 5–37.

4 S. I. Semenova, H. Ohya and K. Soontarapa, Desalination, 1997, 110, 251–286.

5 S. Khoonsap and S. Amnuaypanich, J. Membr. Sci., 2011, 367, 182-189.

6 Y. Shirazi, M. A. Tofighy and T. Mohammadi, J. Membr. Sci., 2011, 378, 551-561.

7 B. Bolto, T. Tran, M. Hoang and Z. Xie, Progr. Polym. Sci., 2009, 34, 969-81.

8 P. S. Rachipudi, M. Y. Kariduraganavar, A. A. Kittur and A. M. Sajjan, J. Membr. Sci., 2011, 383, 224–234.

9 Q. G. Zhang, Q. L. Liu, A. M. Zhu, Y. Xiong and L. Ren, J. Membr. Sci., 2009, 335, 68–75.

10 J. W. Rhim, C. K. Yeom and S. W. Kim, J. Appl. Polym. Sci., 1998, 68, 1717–1723.

11 C. K. Yeom and K. H. Lee, J. Membr. Sci., 1996, 109, 257-265.

12 H. G. Premakshi, A. M. Sajjan and M. Y. Kariduraganavar, DOI: 10.1002/app.41248.

13 S. S. Kulkarni, A. A. Kittur, M. I. Aralaguppi and M. Y. Kariduraganavar, J. Appl. Polym. Sci., 2004, 94, 1304–1315.

14 K. Zhou, Q. G. Zhang, G, L. Han, A. M. Zhu and Q. L. Liu, J. Membr. Sci., 2013, 448, 93–101.

15 N. Alghezawi, O. S¸ anli, L. Aras and G. Asman, Chem. Eng. Process., 2005, 44, 51–58.

16 M. Y. Kariduraganavar, J. G. Varghese, S. K. Choudhari and R. H. Olley, Ind. Eng. Chem. Res., 2009, 48, 4002–4013.

17 H. Zhou, R. Shi and W. Jin, Sep. Purif. Technol., 2014, 127, 61–69.

18 A. M. Sajjan, B. K. Jeevan Kumar, A. A. Kittur and M. Y. Kariduraganavar, J. Membr. Sci., 2013, 425–426, 77–88.

19 H. G. Premakshi, K. Ramesh and M. Y. Kariduraganavar, Chem. Eng. Res. Des., 2015, 94, 32–43.

20 F. Peng, F. Pan, H. Sun, L. Lu and Z. Jiang, J. Membr. Sci. DOI: 10.1016/j.memsci.2007.06.008.

21 H. G. Premakshi, A. M. Sajjan and M. Y. Kariduraganavar, J. Mater. Chem. A, 2015, 3, 3952–3961.

22 T. N. Danks, R. C. T. Slade and J. R. Varcoe, J. Mater. Chem., 2003, 13, 712–721.

23 Y. Xiong, J. Fang, Q. H. Zeng and Q. L. Liu, J. Membr. Sci., 2008, 311, 319–325.

24 L. Lei and Y. X. Wang, J. Membr. Sci., 2005, 262, 1–4.

25 J. Fang and P. K. Shen, J. Membr. Sci., 2006, 285, 317–322.

26 Q. G. Zhang, Q. L. Liu, Z. Y. Jiang and Y. Chen, J. Membr. Sci., 2007, 287, 237–245.

27 X. J. Meng, Q. L. Liu, A. M. Zhu and Q. G. Zhang, J. Membr. Sci., 2010, 360, 276–283.

28 S. Singh, A. Jasti, M. Kumar and V. K. Shahi, Polym. Chem., 2010, 1, 1302-1312.

29 A. M. Sajjan, B. K. Jeevan Kumar, A. A. Kittur and M. Y. Kariduraganavar, J. Ind. Eng. Chem., 2013, 19, 427–437.

30 G. Socrates, Infrared Characteristic Group Frequencies, Wiley, New York, 1980.

31 M. Kumar, S. Singh, V. K. Shahi, J. Phys. Chem. B, 2010, 114, 198–206.

32 Y. Xiong, Q. L. Liu, Q. G. Zhang and A. M. Zhu, J. Power Sources, 2008, 183, 447–453.

33 E. D. Wang, T. S. Zhao and W. W. Yang, I. J. Hydrogen Energy, 2010, 35, 2183–2189.

34 M. H. Eikerling and P. Berg, Soft Matter, 2011, **7,** 5976–5990.

35 A. Vishnyakov and A. V. Neimark, J. Phys. Chem. B, 2001, 105, 9586–9594.

36 R. Y. M. Huang and C. K. Yeom, J. Membr. Sci., 1991, 58, 33–47.

37 S. T. Hwang and K. Kammermeyer, Membrane in Separations, Wiley Interscience, NewYork, 1975.

38 A. Yamasaki, T. Iwatsubo, T. Masuoka and K. Mizoguchi, J. Membr. Sci., 1994, 89, 111-117.

39 S. P. Kusumochayo and M. Sudoh, J. Membr. Sci., 1999, 161, 77-83.

40 S. K. Choudhari, H. G. Premakshi and M. Y. Kariduraganavar, Polym. Bull., DOI 10.1007/s00289-015-1515-0.

41 A. M Sajjan, H. G. Premakshi and M. Y. Kariduraganavar, J. Ind. Eng. Chem., 2015, **25**, 151-161.

42 D. H. Weinkauf and D. R. Paul, in Barrier Polymers and Structures, ed. W. J. Koros, ACS Symp. Ser., Washington, DC, 1990, vol. 423, pp. 61-91.

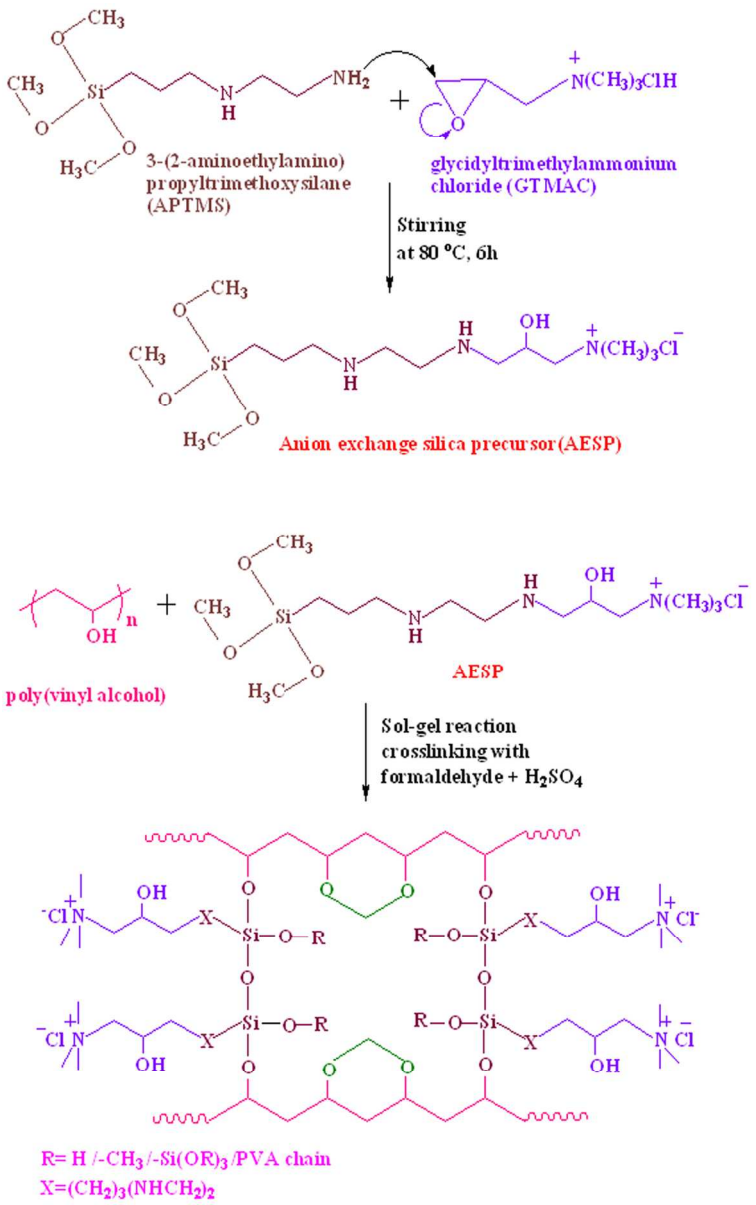

127x203mm (300 x 300 DPI)

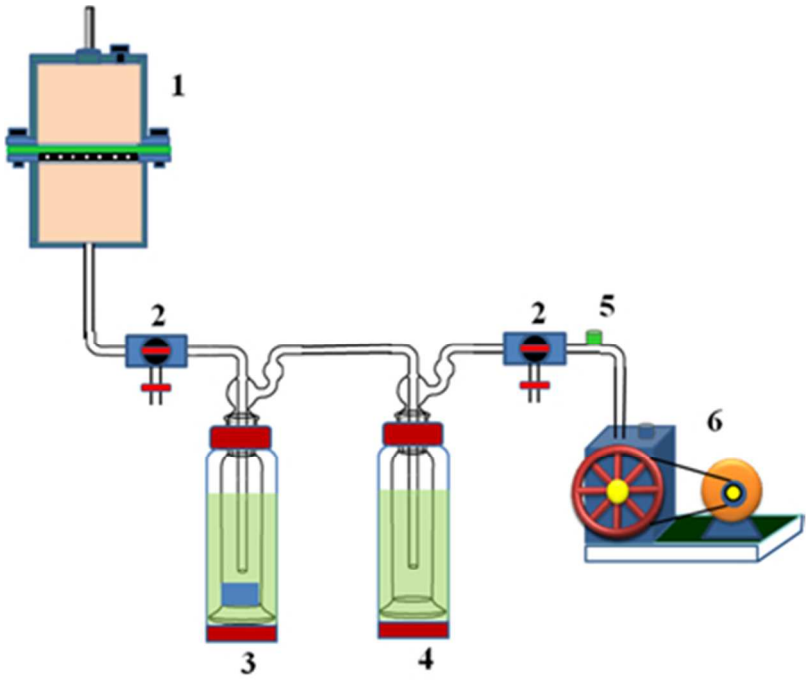

101x85mm (100 x 100 DPI)

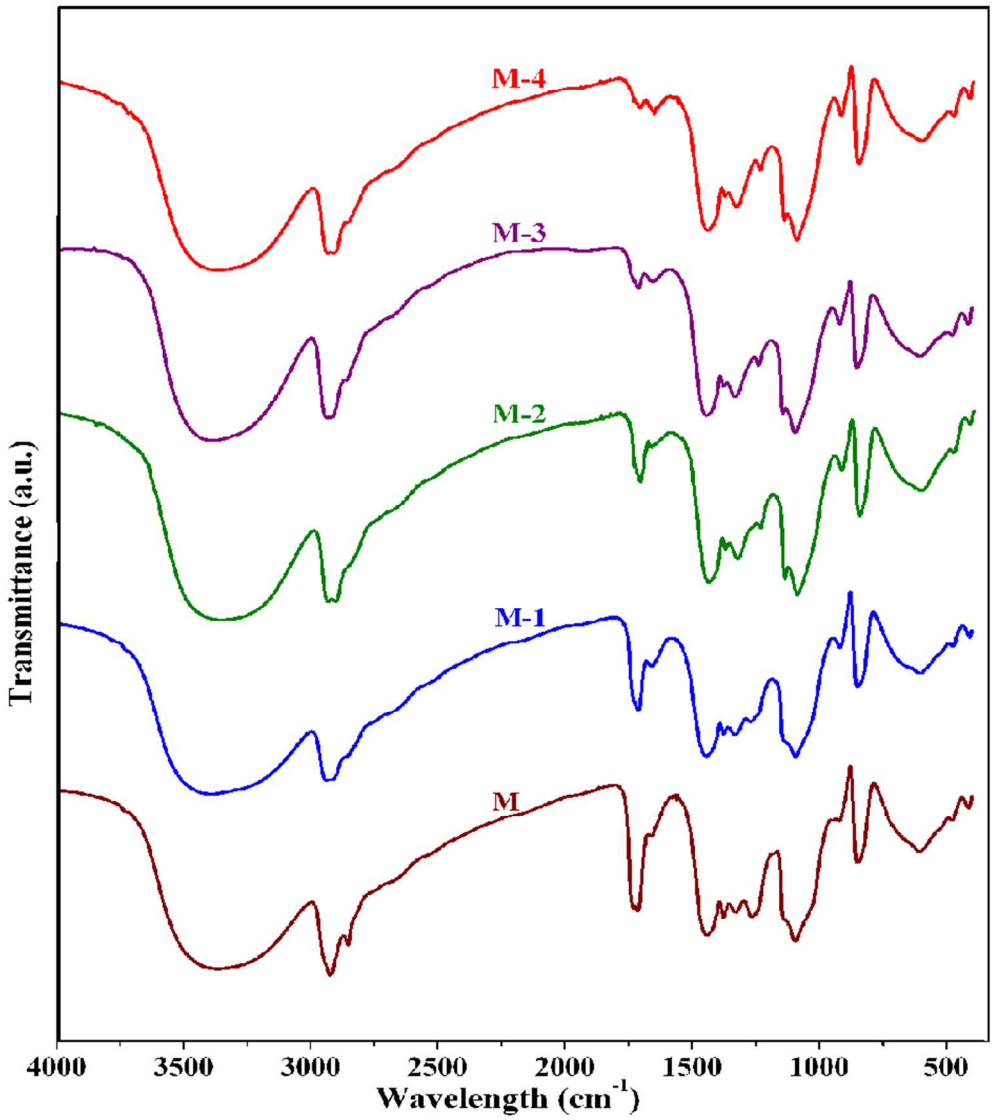

96x109mm (250 x 250 DPI)

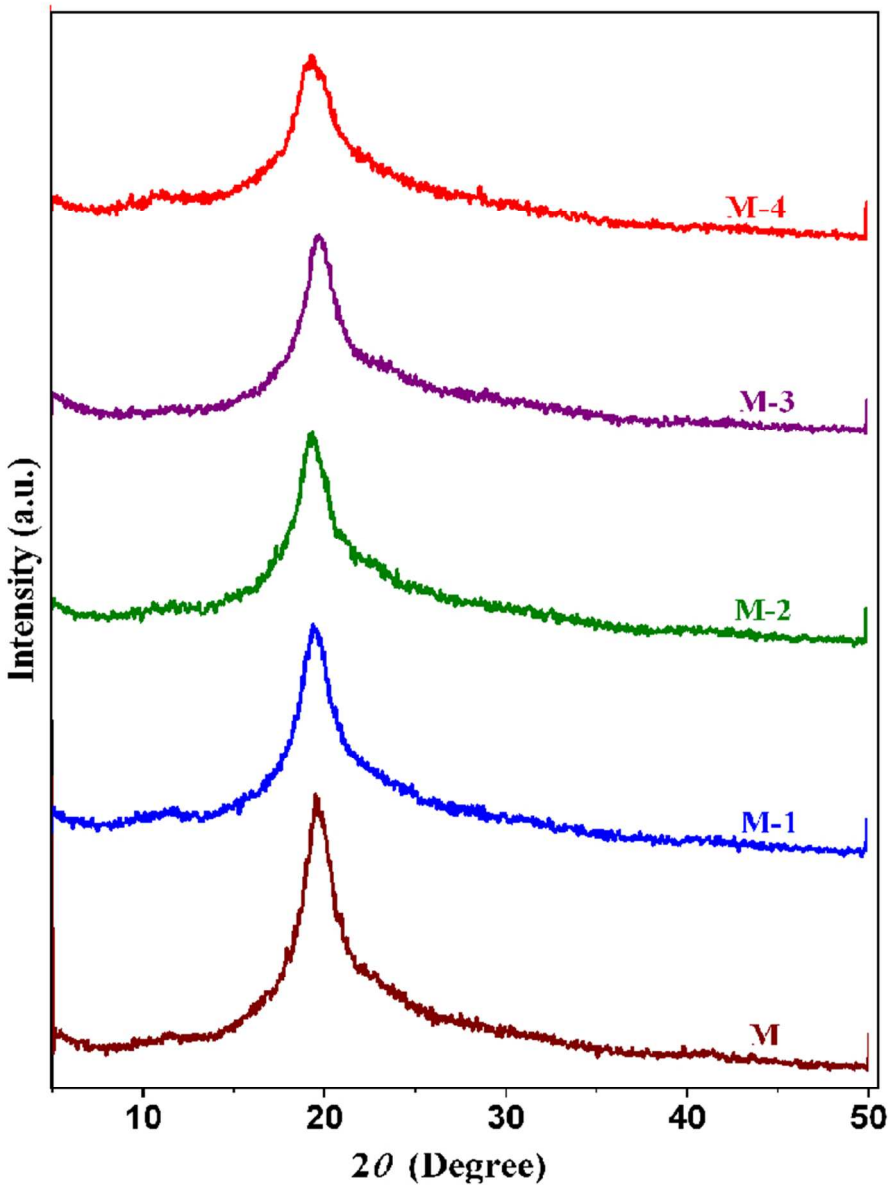

76x101mm (250 x 250 DPI)

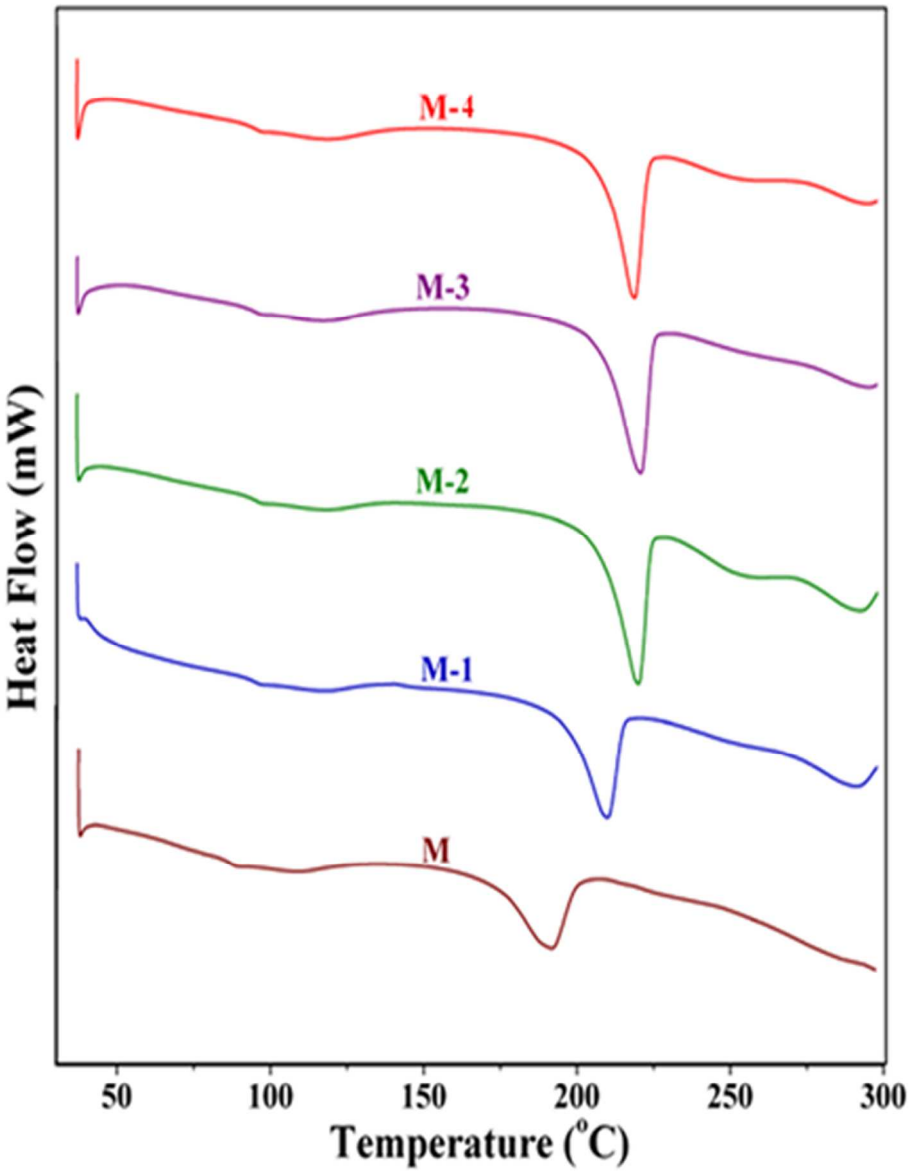
M-4
M-3
M-2
M-1
M
Heat Flow (mW)
50
100
150
200
250
300
Temperature (°C)

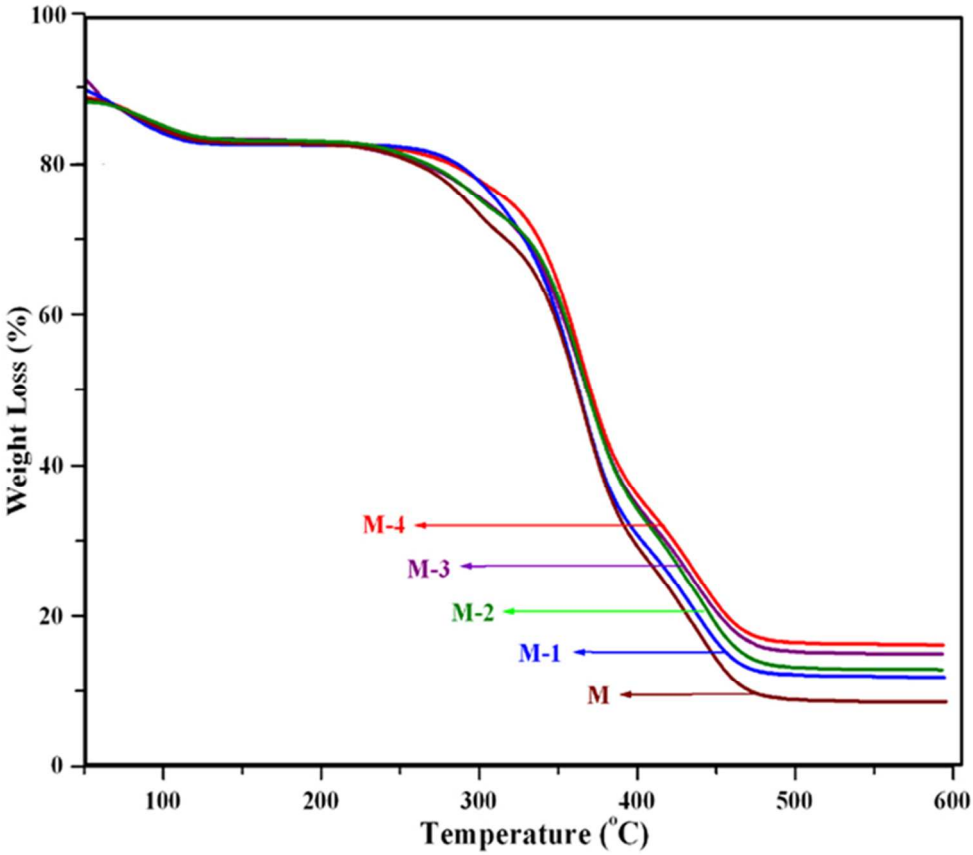

101x88mm (200 x 200 DPI)

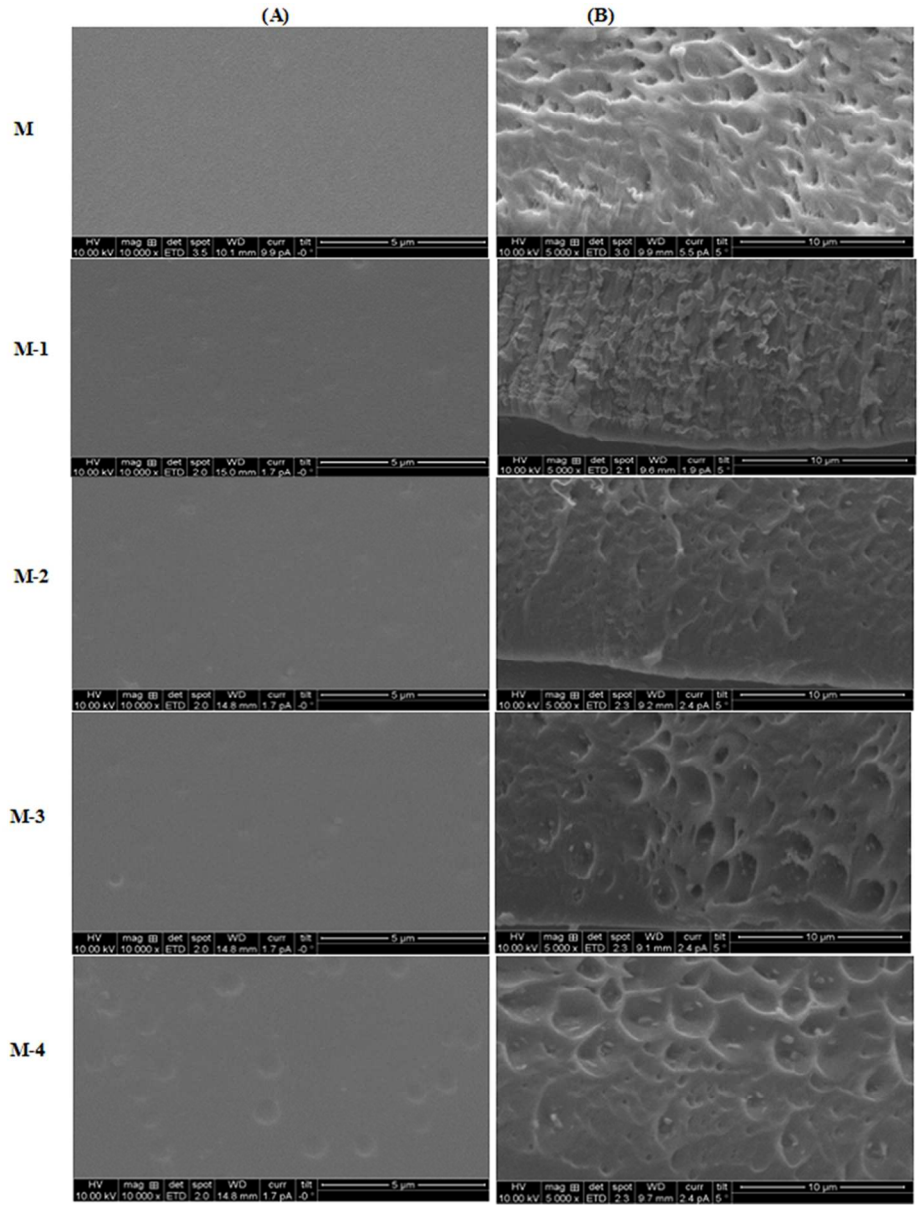
(A)
(B)
M
M-1
M-2
M-3
M-4

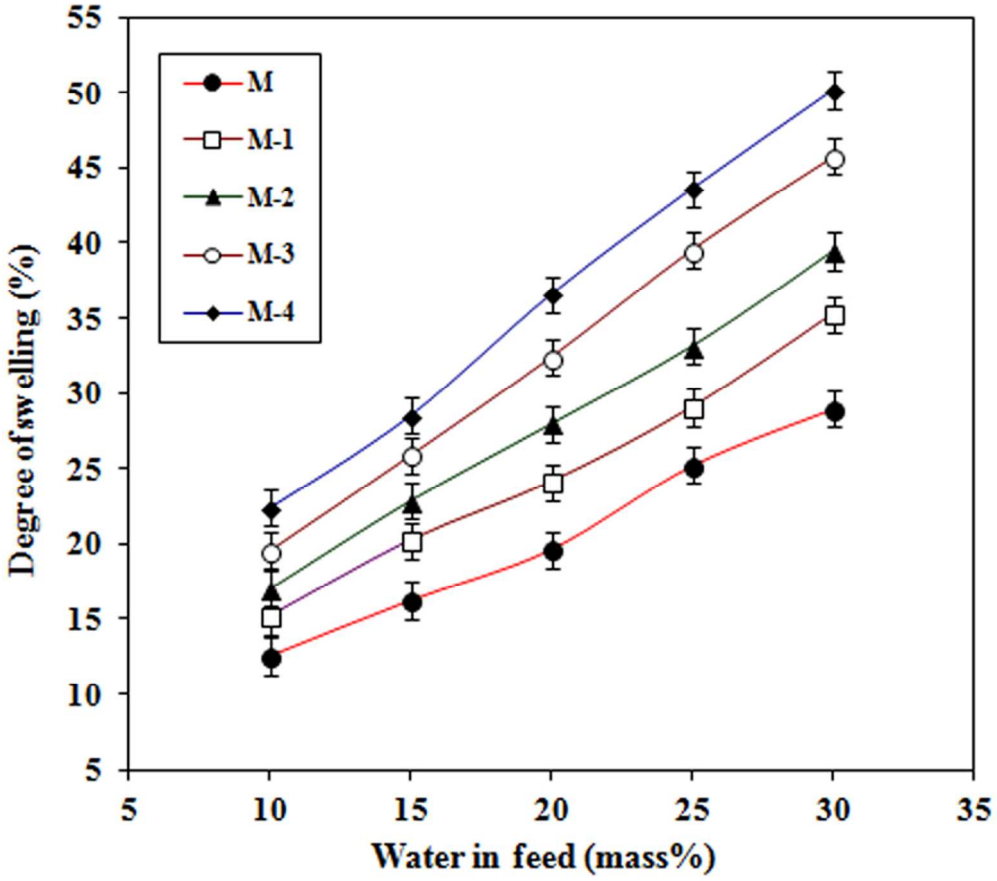
M
M-1
M-2
M-3
M-4
Degree of swelling (%)
Water in feed (mass%)
55
50
45
40
35
30
25
20
15
10
5
5
10
15
20
25
30
35

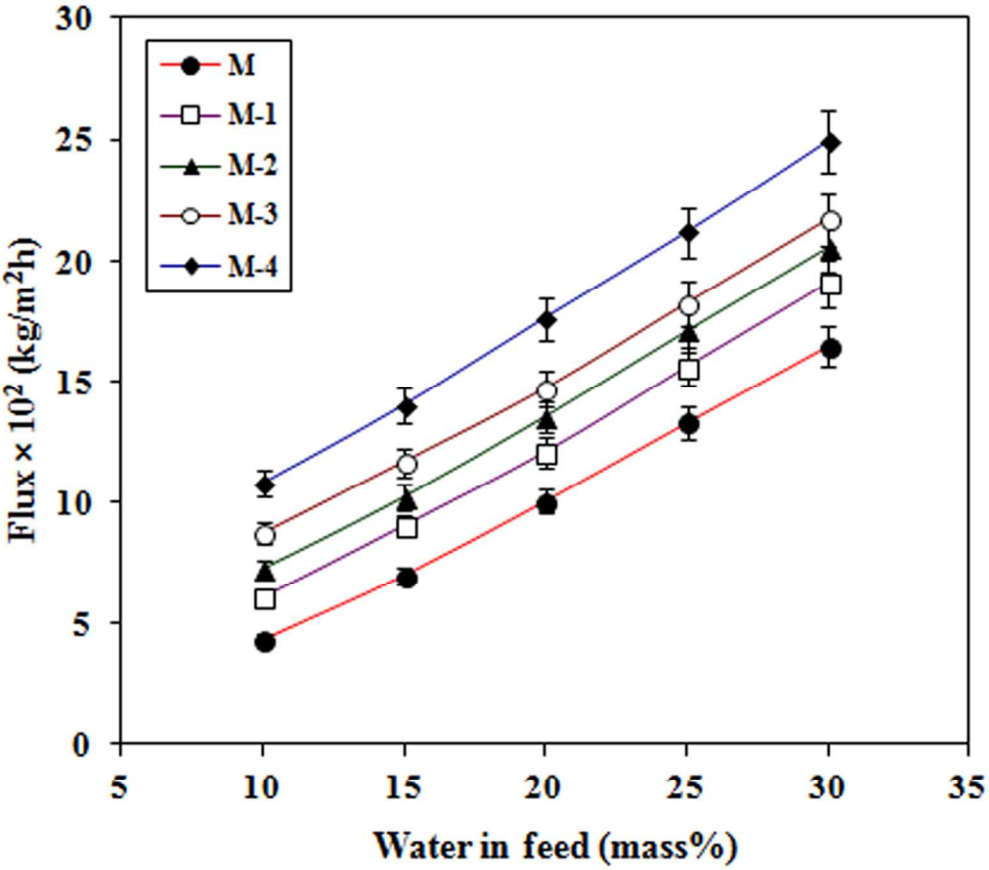
M
M-1
M-2
M-3
M-4
Flux × 10² (kg/m²h)
Water in feed (mass%)
0
5
10
15
20
25
30
5
10
15
20
25
30
35

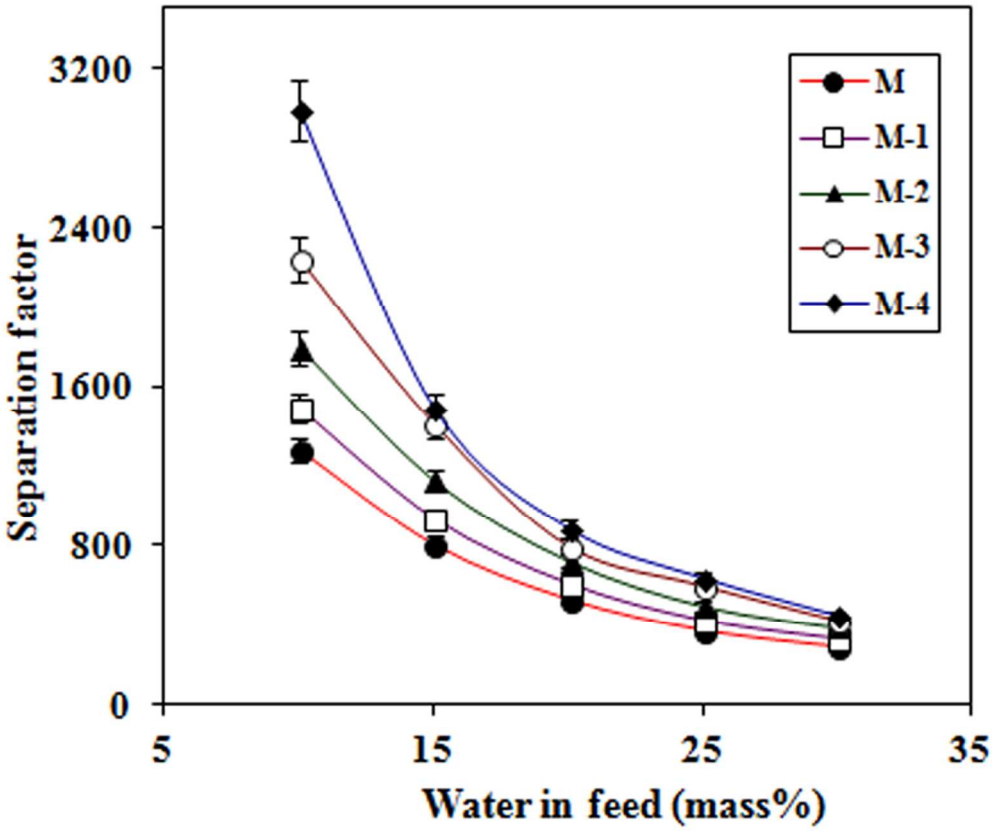
3200
2400
1600
800
0
Separation factor
5
15
25
35
Water in feed (mass%)
M
M-1
M-2
M-3
M-4

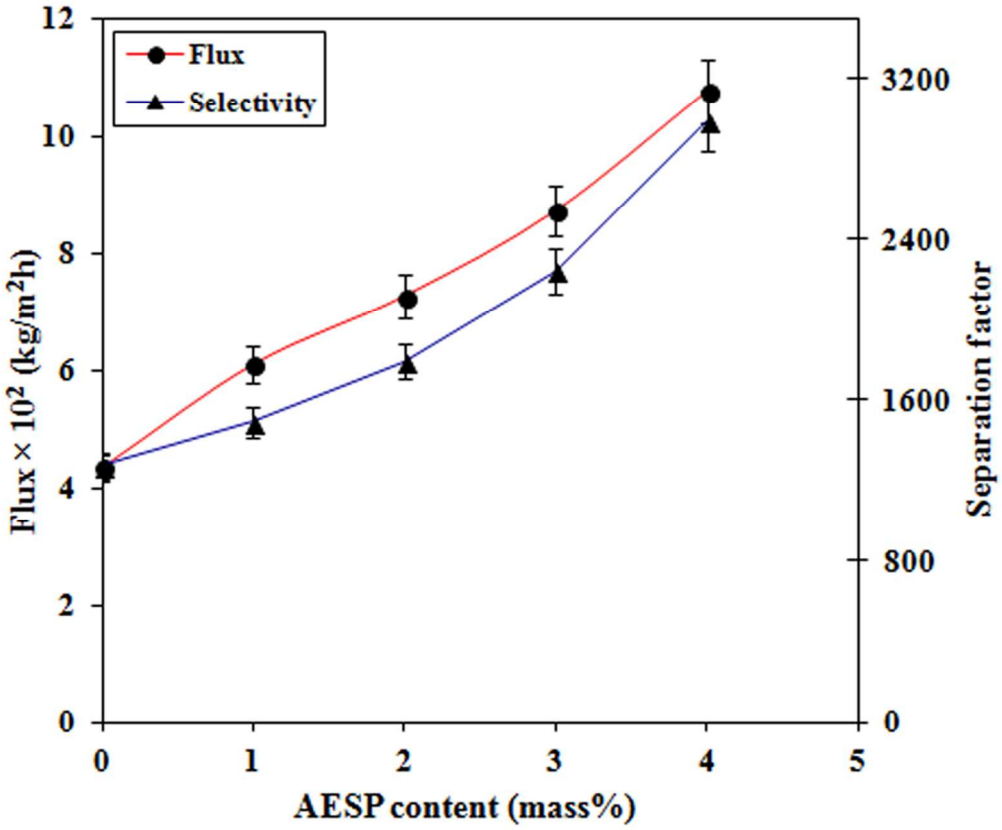
Flux
Selectivity
Flux × 10² (kg/m²h)
Separation factor
AESP content (mass%)
0
2
4
6
8
10
12
0
800
1600
2400
3200
0
1
2
3
4
5

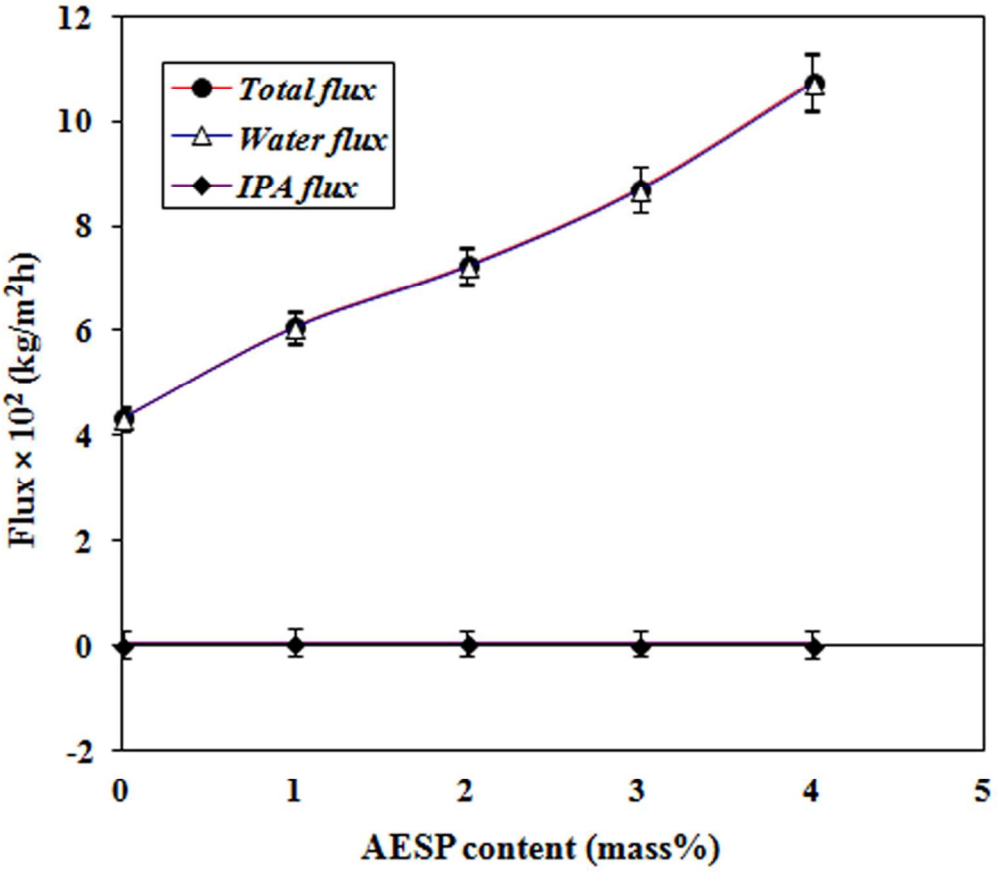
Total flux
Water flux
IPA flux
Flux × 10² (kg/m²h)
AESP content (mass%)
12
10
8
6
4
2
0
-2
0
1
2
3
4
5

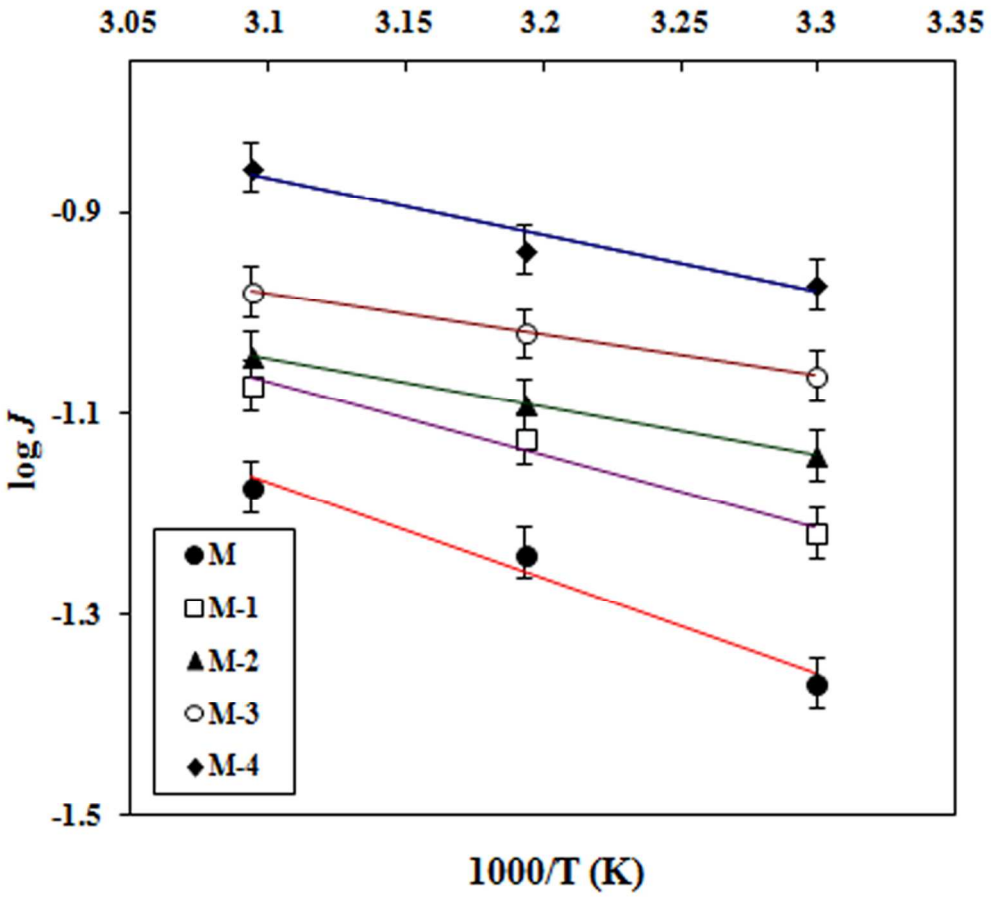
3.05
3.1
3.15
3.2
3.25
3.3
3.35
-0.9
-1.1
-1.3
-1.5
log J
1000/T (K)
M
M-1
M-2
M-3
M-4

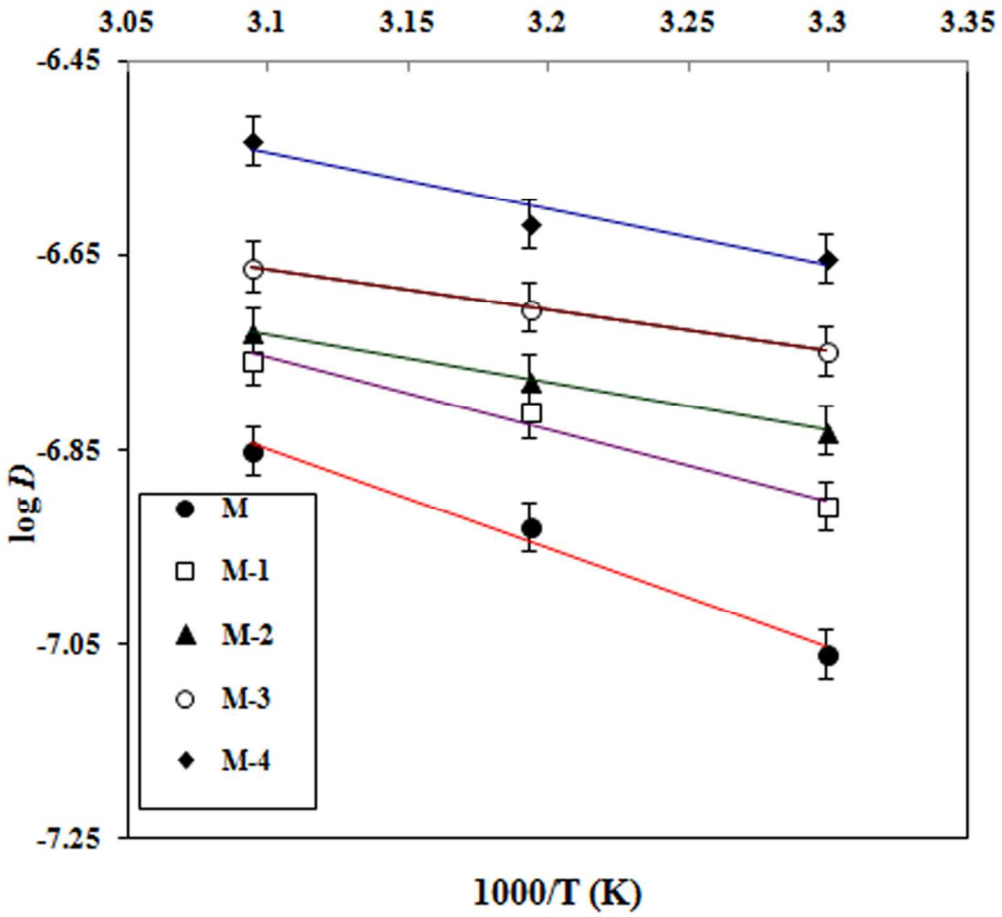
3.05
3.1
3.15
3.2
3.25
3.3
3.35
-6.45
-6.65
-6.85
-7.05
-7.25
log D
1000/T (K)
M
M-1
M-2
M-3
M-4

FIGURE CAPTIONS

Fig. 1 Development of composite anion exchange membrane.

Fig. 2 Schematic representation of pervaporation apparatus: (1) pervaporation cell; (2) vacuum control valves; (3) permeate cold trap; (4) moisture cold trap; (5) pressure sensor; (6) vacuum pump.

Fig. 3 FTIR spectra of crosslinked PVA and its composite anion-exchange membranes: (M) 0 mass%; (M-1) 1 mass%; (M-2) 2 mass%; (M-3) 3 mass%; (M-4) 4 mass% of AESP.

Fig. 4 Wide-angle X-ray diffraction patterns of crosslinked PVA and its composite anion exchange membranes: (M) 0 mass%; (M-1) 1 mass%; (M-2) 2 mass%; (M-3) 3 mass%; (M-4) 4 mass% of AESP.

Fig. 5 DSC thermograms of crosslinked PVA and its composite anion exchange membranes: (M) 0 mass%; (M-1) 1 mass%; (M-2) 2 mass%; (M-3) 3 mass%; (M-4) 4 mass% of AESP.

Fig. 6 Thermogravimetric analysis of crosslinked PVA and its composite anion exchange membranes: (M) 0 mass%; (M-1) 1 mass%; (M-2) 2 mass%; (M-3) 3 mass%; (M-4) 4 mass% of AESP.

Fig. 7 SEM micrographs of crosslinked PVA and its composite anion exchange membranes: (A) surface views and (B) cross-sectional views.

Fig. 8 Variation of degree of swelling with different mass% of water in the feed for crosslinked PVA and its composite anion exchange membranes.

Fig. 9 Variation of total pervaporation flux with different mass% of water in the feed for crosslinked PVA and its composite anion exchange membranes.

Fig. 10 Variation of separation factor with different mass% of water in the feed for crosslinked PVA and its composite anion exchange membranes.

Fig. 11 Variation of total flux and separation factor with different mass% of AESP in the membranes at 10 mass% of water in the feed.

Fig. 12 Variation of total flux, and fluxes of water and isopropanol with different mass% of AESP in the membranes at 10 mass% of water in the feed.

Fig. 13 Variation of log J with temperature for crosslinked PVA and its composite anion exchange membranes at 10 mass% of water in the feed.

Fig. 14 Variation of log D with temperature for crosslinked PVA and its composite anion exchange membranes at 10 mass% of water in the feed.

Table 1 Mechanical properties and ion-exchange capacity of crosslinked PVA and its composite membranes.

Membrane	Tensile strength (MPa)	Elongation at Break (%)	*IEC* (meq/g)
M	54±1.08	90±1.24	0.00±00
M-1	55±2.60	80±1.08	0.25±0.08
M-2	58±1.10	56±2.30	0.40±0.06
M-3	62±1.68	50±2.34	0.62±0.05
M-4	69±3.25	45±2.73	0.73±0.07

Table 2 Diffusion coefficients of water and isopropanol at different mass% of water in the feed for different membranes.

Mass % of water	$D_w \times 10^8$ (cm^2/s)					$D_{IPA} \times 10^{10}$ (cm^2/s)				
	M	M-1	M-2	M-3	M-4	M	M-1	M-2	M-3	M-4
5	8.74 ±0.42	12.40 ±0.63	14.83 ±0.74	17.92 ±0.84	22.35 ±0.95	2.71 ±0.08	2.69 ±0.08	2.59 ±0.07	2.40 ±0.06	2.25 ±0.04
10	9.02 ±0.44	12.30 ±0.60	13.91 ±0.71	15.91 ±0.79	19.26 ±0.90	4.40 ±0.16	4.26 ±0.15	4.01 ±0.13	3.85 ±0.12	3.67 ±0.11
15	10.1 ±0.52	12.22 ±0.59	13.82 ±0.68	15.00 ±0.78	18.14 ±0.89	6.62 ±0.27	6.55 ±0.26	6.28 ±0.23	6.22 ±0.22	6.14 ±0.21
20	10.00 ±0.49	12.14 ±0.58	13.90 ±0.70	14.90 ±0.76	17.45 ±0.86	9.73 ±0.51	9.46 ±0.48	9.12 ±0.45	8.86 ±0.41	8.12 ±0.31
25	11.1 ±0.55	12.01 ±0.56	13.91 ±0.71	14.81 ±0.73	17.01 ±0.81	12.70 ±0.68	12.60 ±0.65	12.40 ±0.60	11.80 ±0.59	12.4 ±0.61

Table 3 Pervaporation flux and separation selectivity for different membranes at different temperatures for 10 mass% of water in the feed.

Temp.°C	Jx10^2 (kg/m^{2}h)					α_{sep}				
	M	M-1	M-2	M-3	M-4	M	M-1	M-2	M-3	M-4
30	4.34 ±0.12	6.09 ±0.23	7.26 ±0.29	8.72 ±0.41	10.76 ±0.56	1277 ±39	1491 ±53	1791 ±62	2242 ±75	2991 ±98
40	5.83 ±0.18	7.58 ±0.30	8.17 ±0.32	9.63 ±0.47	11.67 ±0.59	1190 ±35	1277 ±40	1376 ±42	1492 ±55	1793 ±66
50	6.80 ±0.25	8.55 ±0.34	9.13 ±0.43	10.59 ±0.53	14.10 ±0.64	1116 ±32	1188 ±34	1275 ±40	1276 ±41	1489 ±51

Table 4 Arrhenius activation parameters for permeation and diffusion, and heat of sorption.

Parameters (kJ/mol)	M	M-1	M-2	M-3	M-4
E_p	18.36	13.86	10.95	9.36	7.94
E_D	18.68	14.12	11.26	9.54	8.09
Epw	18.32	13.80	10.82	9.28	7.81
EpIPA	22.98	23.15	23.81	30.83	39.31
ΔH_s	-0.32	-0.26	-0.31	-0.18	-0.15

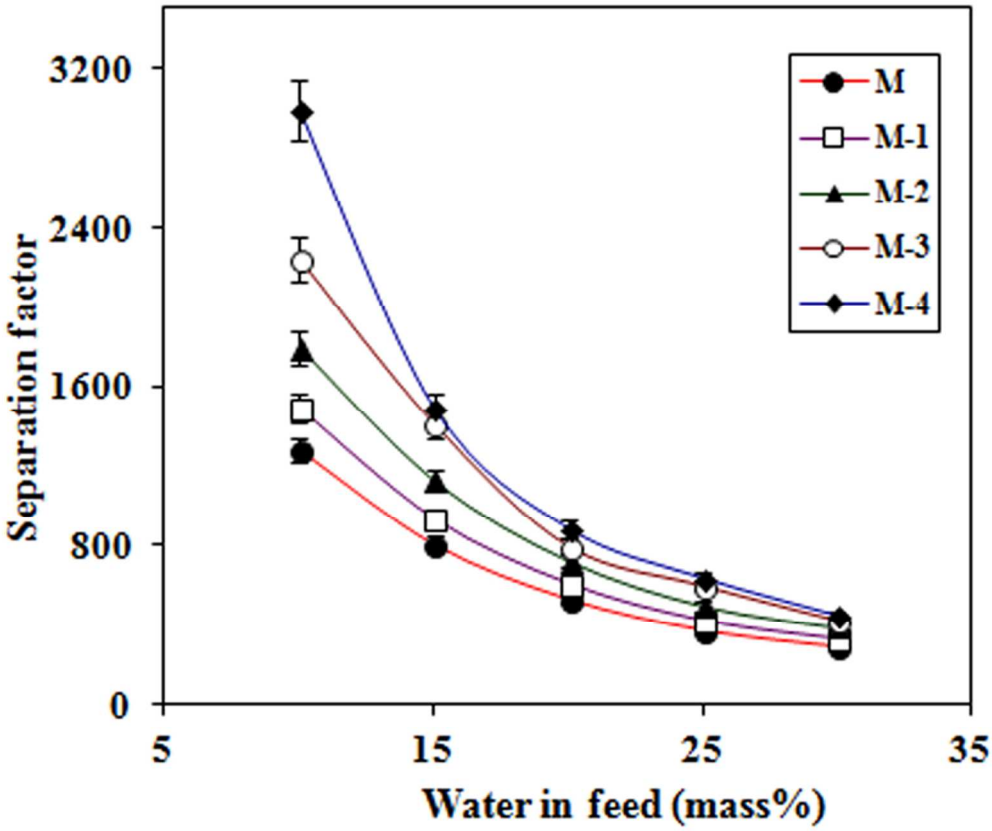
3200
2400
1600
800
0
Separation factor
5
15
25
35
Water in feed (mass%)
M
M-1
M-2
M-3
M-4